



Associated Z' production in the flavorful $U(1)$ scenario for $R_{K^{(*)}}$

Siddharth Dwivedi^{1,a}, Adam Falkowski^{2,b}, Dilip Kumar Ghosh^{1,c}, Nivedita Ghosh^{1,d}

¹ School of Physical Sciences, Indian Association for the Cultivation of Science, 2A & 2B, Raja S.C. Mullick Road, Kolkata 700032, India

² Laboratoire de Physique Théorique (UMR8627), CNRS, Univ. Paris-Sud, Université Paris-Saclay, 91405 Orsay, France

Received: 5 September 2019 / Accepted: 5 March 2020 / Published online: 23 March 2020
© The Author(s) 2020

Abstract The flavorful Z' model with its couplings restricted to the left-handed second generation leptons and third generation quarks can potentially resolve the observed anomalies in R_K and R_{K^*} . After examining the current limits on this model from various low-energy processes, we probe this scenario at 14 TeV high-luminosity run of the LHC using two complementary channels: one governed by the coupling of Z' to b -quarks and the other to muons. We also discuss the implications of the latest LHC high mass resonance searches in the dimuon channel on the model parameter space of our interest.

1 Introduction

In the last few years, the LHCb collaboration has reported a number of deviations from μ - e universality in B-meson processes. In particular, the ratios of $\mu^+\mu^-$ to e^+e^- final states in $B \rightarrow K^{(*)}\ell^+\ell^-$ decays: R_K [1] and R_{K^*} [2] are observed to be smaller than one, each displaying a $\sim 2.5\sigma$ deviation from lepton-flavor universality predicted by the Standard Model (SM). Recent global analyses [3–7], which also take into account other $b \rightarrow s\ell^+\ell^-$ mediated processes, conclude that the SM is disfavored by the current experimental data with a confidence level exceeding 5σ .

The global fit can be significantly improved if the effective Lagrangian below the weak scale contains new contributions to the 4-fermion operator $(\bar{b}_L\gamma^\rho s_L)(\bar{\mu}_L\gamma_\rho\mu_L)$, in addition to the ones generated by the exchange of SM particles in loops. One option to arrange for these contributions is to assume that the high-energy theory contains a new electrically neutral vector particle Z' coupled to muons and, in a flavor-violating way, to bottom and strange quarks. In this scenario,

the 4-fermion operator in question can arise from tree-level Z' exchange. There is already a vast literature discussing Z' models explaining the $b \rightarrow s\ell\ell$ anomalies, see e.g. [8–47]. A generic feature of these model is that the Z' is within the kinematic reach of the LHC and thus can be searched for directly. In particular, these models always predict a non-zero cross section for the quark-level process $b(\bar{b})\bar{s}(s) \rightarrow Z' \rightarrow \mu\mu$, which leads to the dimuon resonance signature at the LHC. Furthermore, in some models the Z' coupling to bs is correlated with couplings to other quarks, which opens further production channels at the LHC [27, 32].

The goal of this paper is to study new LHC signatures of the Z' boson responsible for the $b \rightarrow s\ell\ell$ anomalies. We consider the model described in Ref. [37] where Z' , in addition to the coupling to muons, also possesses a sizable coupling to $b\bar{b}$. This model predicts several new signatures where Z' is produced in association with some SM particles. We focus on two such signatures, which we find especially promising:

- $pp \rightarrow Z' + 1b(2b) \rightarrow \mu^+\mu^- + 1b(2b)$,
- $pp \rightarrow Z'\mu^\pm + \cancel{E}_T \rightarrow 3\mu + \cancel{E}_T$.

For these two processes we study the discovery prospects at the LHC run 3 and the subsequent high-luminosity phase (HL-LHC). We show that the above signature can be observed with the significance exceeding 5σ in the parameter space of the Z' model favored by the $b \rightarrow s\ell\ell$ anomalies and consistent with all other experimental constraints. The information obtained by studying these two processes is complementary to that conveyed by generic dimuon resonance searches, and will be crucial for the identification of the microscopic model responsible for the $b \rightarrow s\ell\ell$ anomalies.

In what follows, in Sect. 2 we discuss the model and list the range of couplings of the Z' to muons and b -quarks allowed by low-energy precision measurements. In Sect. 3 we present a detailed analysis of LHC prospects of discovering the Z' in two complementary channels where the Z' is produced in association with SM particles. The production rate of Z'

^a e-mail: tpsd5@iacs.res.in

^b e-mail: adam.falkowski@th.u-psud.fr

^c e-mail: tpdkg@iacs.res.in

^d e-mail: tpng@iacs.res.in (corresponding author)

in the two channels is governed by its coupling either to b -quarks or to muons and thus they can potentially probe different regions of the allowed parameter space dominated by either of the two couplings. In Sect. 4 we compare the sensitivity of these associated Z' production searches with that of the generic dimuon resonance searches. Finally, we summarise and conclude in Sect. 5.

2 The model

We consider a massive spin-1 boson Z' with coupling to quarks and leptons that can address the R_K and R_{K^*} anomalies. We work with the setup described in Ref. [37], however in this paper we assume that only the Z' boson can be produced at the energy scale available at the LHC. The relevant BSM interactions pertaining to our collider analysis are encoded in the following Lagrangian:

$$\mathcal{L} \supset Z'_\mu (g_{bb}\bar{q}_L\gamma^\mu q_L + g_{bs}\bar{b}_L\gamma^\mu s_L + g_{\mu\mu}\bar{L}_L\gamma^\mu L_L), \tag{2.1}$$

where $q_L = (t_L, b_L)^T, L_L = (\nu_{\mu L}, \mu_L)^T$. The Z' couplings $g_{\mu\mu}, g_{bb}$, and g_{bs} to muons, s - and b -quarks are in principle free parameters. However, in the setup of [37] in the absence of fine-tuning one expects $|g_{bs}| \sim |V_{ts}g_{bb}|$, where $|V_{ts}| \approx 0.04$ is the 3-2 entry of the CKM matrix. In the following for simplicity we assume $g_{bs} = V_{ts}g_{bb}$, and that g_{bb} and $g_{\mu\mu}$ have the same sign. Thus, the parameter space in our analysis is 3-dimensional, and consists of the 2 couplings $g_{bb}, g_{\mu\mu}$ and the Z' mass $M_{Z'}$.

Integrating out the Z' boson generates four-fermion contact interactions in the effective theory below the scale $M_{Z'}$. In particular, a new contribution to the effective interaction $(\bar{b}_L\gamma_\rho s_L)(\bar{\mu}_L\gamma^\rho \mu_L)$ is generated, adding to the SM contribution induced at the loop level. This is the scenario with $C_{9\mu}^{\text{NP}} = -C_{10\mu}^{\text{NP}}$, using the standard notation of flavor physics. Such a pattern of new physics corrections provides a very good fit to the measured R_K, R_{K^*} , and other $b \rightarrow s\mu\mu$ observables [3–7]. The best fit of Ref. [5], $C_{9\mu}^{\text{NP}} = -C_{10\mu}^{\text{NP}} = -0.53 \pm 0.09$, translates into the following constraint on our parameters:

$$\frac{g_{bb}g_{\mu\mu}}{M_{Z'}^2} = \frac{1.00 \pm 0.17}{(6.9 \text{ TeV})^2} \quad @ 68\% \text{ CL}. \tag{2.2}$$

In the following of this analysis we will assume that the values of the parameters correspond to this best fit within 1σ uncertainty.

There are further low-energy constraints on these parameters. One is due to four-lepton interactions generated by integrating out Z' , which are constrained by the trident muon production in neutrino scattering [48–50]. Using the global fit of Ref. [51] one finds

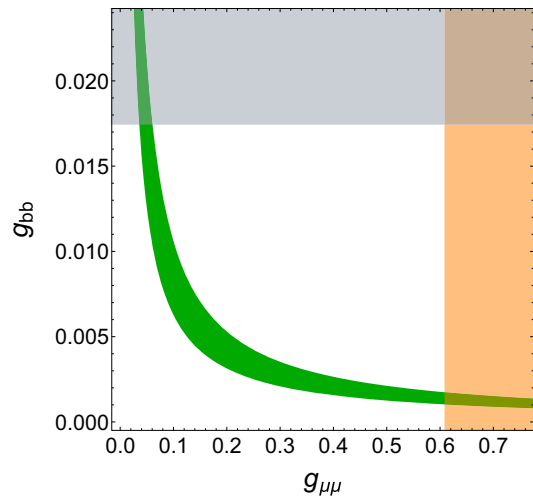


Fig. 1 The parameter space in the $(g_{\mu\mu}, g_{bb})$ plane for $M_{Z'} = 200 \text{ GeV}$ preferred at 68% CL by the $b \rightarrow s\ell^+\ell^-$ anomalies (parabolic green band). We also show the regions excluded at 99% CL by trident neutrino production (vertical orange band), and by the analysis Ref. [53] comparing the Δm_{B_s} and $B \rightarrow D^{*\ell\nu}$ probes of the CKM elements (horizontal grey band)

$$\frac{g_{\mu\mu}^2}{M_{Z'}^2} \lesssim \frac{1}{(330 \text{ GeV})^2} \quad @ 99\% \text{ CL}. \tag{2.3}$$

Another combination of the model parameters is probed thanks to the Z' generating the $\Delta F = 2$ operator $(\bar{b}_L\gamma_\mu s_L)^2$, which affects the B_s meson mass difference Δm_{B_s} . In some of the previous literature this contribution is constrained by comparing the experimentally measured Δm_{B_s} with the one predicted by the SM. This is however not quite correct. The reason is that the SM prediction $\Delta m_{B_s}^{\text{SM}}$ is a function of the CKM parameters, which are obtained from a global fit to flavor observables (see e.g. [52]). *These fits always include the B_s meson mass difference as one of the inputs.* As a result, the CKM parameters and consequently the predicted $\Delta m_{B_s}^{\text{SM}}$ can be “contaminated” by the new physics contribution of the Z' , and it is not consistent to use the Δm_{B_s} observable alone to constrain Z' . Instead, consistent constraints can be obtained by comparing *different* observables that probe the same CKM parameters but are affected *differently* by the Z' . Such an analysis was performed in Ref. [53] which compared CKM parameters extracted from Δm_{B_s} with those extracted from $B \rightarrow D^{(*)}\ell\nu$ decays. That analysis leads to the constraint

$$\frac{g_{bb}^2}{M_{Z'}^2} \lesssim \frac{1}{(11.5 \text{ TeV})^2} \quad @ 99\% \text{ CL}. \tag{2.4}$$

An example of the parameter space is shown in Fig. 1 for $M_{Z'} = 200 \text{ GeV}$. Clearly, fitting the $b \rightarrow s\mu\mu$ anomalies together with the low-energy constraints discussed above leaves a finite interval for the Z' coupling $g_{\mu\mu}$ and g_{bb} . The intervals $g_{\mu\mu}^{\text{min}} \lesssim g_{\mu\mu} \lesssim g_{\mu\mu}^{\text{max}}$ and $g_{bb}^{\text{min}} \lesssim g_{bb} \lesssim g_{bb}^{\text{max}}$

Table 1 Intervals for the couplings $g_{\mu\mu}$ and g_{bb} consistent with explaining the $b \rightarrow s\ell\ell$ anomalies, and not excluded at 99% CL by the CKM [53] and trident [50] constraints. We also show the 1σ confidence interval for the coupling $g_{\mu\mu}$ obtained from the likelihood combining the above mentioned constraints

$M_{Z'}$ (GeV)	$g_{\mu\mu}^{\min}$	$g_{\mu\mu}^{\max}$	$g_{\mu\mu}^{1\sigma}$	g_{bb}^{\min}	g_{bb}^{\max}
200	0.040	0.61	[0.067, 0.078]	0.0016	0.017
300	0.060	0.91	[0.10, 0.12]	0.0024	0.026
500	0.10	1.5	[0.16, 0.20]	0.0040	0.044
750	0.15	2.3	[0.24, 0.32]	0.0060	0.065
1000	0.20	3.0	[0.32, 0.43]	0.0080	0.087

allowed at 99% CL for the particular values of $M_{Z'}$ used in our collider analysis are shown in Table 1.

3 Collider analysis

In this section we discuss LHC signatures of a Z' boson with a pattern of couplings to matter motivated by the $b \rightarrow s\mu\mu$ anomalies, as given in Eq. (2.1). One signature, already discussed in several previous works [32, 37], is the resonant dimuon production, $pp \rightarrow Z' \rightarrow \mu^+\mu^-$. In this scenario, the Z' is predominantly produced at the LHC via the $b\bar{b}$ fusion, with a subleading contribution from the $b\bar{s}$ and $\bar{b}s$ fusion, and it decays to a pair of muons with a branching fraction that is strongly dependent on the couplings g_{bb} and $g_{\mu\mu}$. Another signature is $pp \rightarrow Z \rightarrow 4\mu$ [10, 50, 54], where the Z boson first decays to two muons, and then a Z' (off-shell or on-shell, depending on its mass) is radiated off one of the muons.

The goal of this paper is to explore alternative signatures of the Z' boson at the LHC. We focus on the following two processes:

- $pp \rightarrow Z' + 1b(2b) \rightarrow \mu^+\mu^- + 1b(2b)$,
- $pp \rightarrow Z'\mu^\pm \cancel{E}_T \rightarrow 3\mu^\pm + \cancel{E}_T$.

The leading Feynman diagrams for these processes are shown in Figs. 2 and 3. In the first process the Z' boson is radiated off a b -quark, while in the second it is radiated off a muon or a neutrino. In both cases we study the situation where the Z' decays to a muon pair. Consequently, the rate of the first process depends on both g_{bb} and $g_{\mu\mu}$ couplings, while in the second case it depends only on $g_{\mu\mu}$. Note that, following Eq. (2.2), the magnitude of g_{bb} and $g_{\mu\mu}$ is anti-correlated in our scenario. For this reason, the two processes target complementary regions of the parameter space: the $3\mu^\pm + \cancel{E}_T$ signal is more relevant for larger $g_{\mu\mu}$, while the $\mu^+\mu^- + b$ signal is more relevant for smaller $g_{\mu\mu}$.

We implemented the interactions in Eq. (2.1) in FeynRules [55] so as to generate a MadGraph5 model

file. We then generated both the signal as well as SM backgrounds events using MadGraph5_aMC@NLO [56] at the leading order (LO) and at the parton level. For the parton distribution function (PDF) we used the NN23LO1 implementation [57]. The parton level events are passed to PYTHIA 8 [58] for showering and hadronization. Finally, the showered events are passed through the detector level simulation using Delphes3 [59], with the jets reconstructed using the anti- k_T jet algorithm [60]. In our analysis we ignore Z' production proceeding via the $Z'-b-s$ coupling, which is suppressed due to the smallness of that coupling in our model, $g_{bs}/g_{bb} \sim |V_{ts}| = \mathcal{O}(10^{-2})$.

3.1 $pp \rightarrow Z' + 1b(2b) \rightarrow \mu^+\mu^- + 1b(2b)$ channel

In this channel we consider the production of the Z' boson in $\sqrt{s} = 14$ TeV LHC in association with either one or two b -quarks, followed by the Z' decay into a muon pair. The dominant background contributions for this signal arise from the SM processes $pp \rightarrow \mu^+\mu^- + jets$, $pp \rightarrow t\bar{t} + jets \rightarrow b\bar{b}W^+W^- + jets \rightarrow b\bar{b}\mu^+\mu^- \nu_\mu\bar{\nu}_\mu + jets$. Here $jets$ denote both the light jets and b -jets. The light jets are taken into account since they can contribute to the background via being mistagged as b -jets. For the $\mu^+\mu^- + jets$ and for $t\bar{t} + jets$ background, events are matched up to three jets and two jets respectively by kt-MLM matching scheme [61, 62].

To generate our signal and background events, we employ the following preselection cuts:

$$\begin{aligned} \Delta R_{jj,bb,bl,jl} &> 0.4, \quad \Delta R_{\ell\ell} > 0.2, \\ p_T(j, b, \ell) &> 10 \text{ GeV}, \quad |\eta_{j,b,\ell}| < 2.5. \end{aligned} \tag{3.1}$$

After implementing these cuts, the dependence of the signal cross section on the coupling $g_{\mu\mu}$ is shown in Fig. 4 for $M_{Z'} = 200, 500$ and 1000 GeV. In our simulations, for a given $g_{\mu\mu}$ and $M_{Z'}$, the value of g_{bb} is fixed to the central value determined from Eq. (2.2). The upper and lower ends of each signal cross-section curve are due to the finite allowed range of the couplings g_{bb} and $g_{\mu\mu}$ as shown in Table 1.

We require the final state to be comprised of two oppositely charged muons and one or two b -tagged jets with $p_T(b) > 20$ GeV. We also impose an electron veto in the final state. The requirement of b -tagged jets helps to reduce the $\mu^+\mu^- + jets$ background. The p_T dependent b -tag efficiency (ϵ_b) for the b -jets is $\epsilon_b = 0.85 \tanh(0.0025 p_T) \left(\frac{25.0}{1 + 0.063 p_T} \right)$. The misidentification efficiency functions for the c -jets (ϵ_c) and that of the other light quark and gluon jets (ϵ_j) have the form, $\epsilon_c = 0.25 \tanh(0.018 p_T) \left(\frac{1}{1 + 0.0013 p_T} \right)$ and $\epsilon_j = 0.01 + 0.000038 p_T$, respectively [63].

To further optimize the signal selection cuts, we study the distributions of selected kinematic variables. First, we study the transverse momentum distributions of the two muons. In

Fig. 2 Leading Feynman diagrams for the $Z' + 1b(2b)$ final state

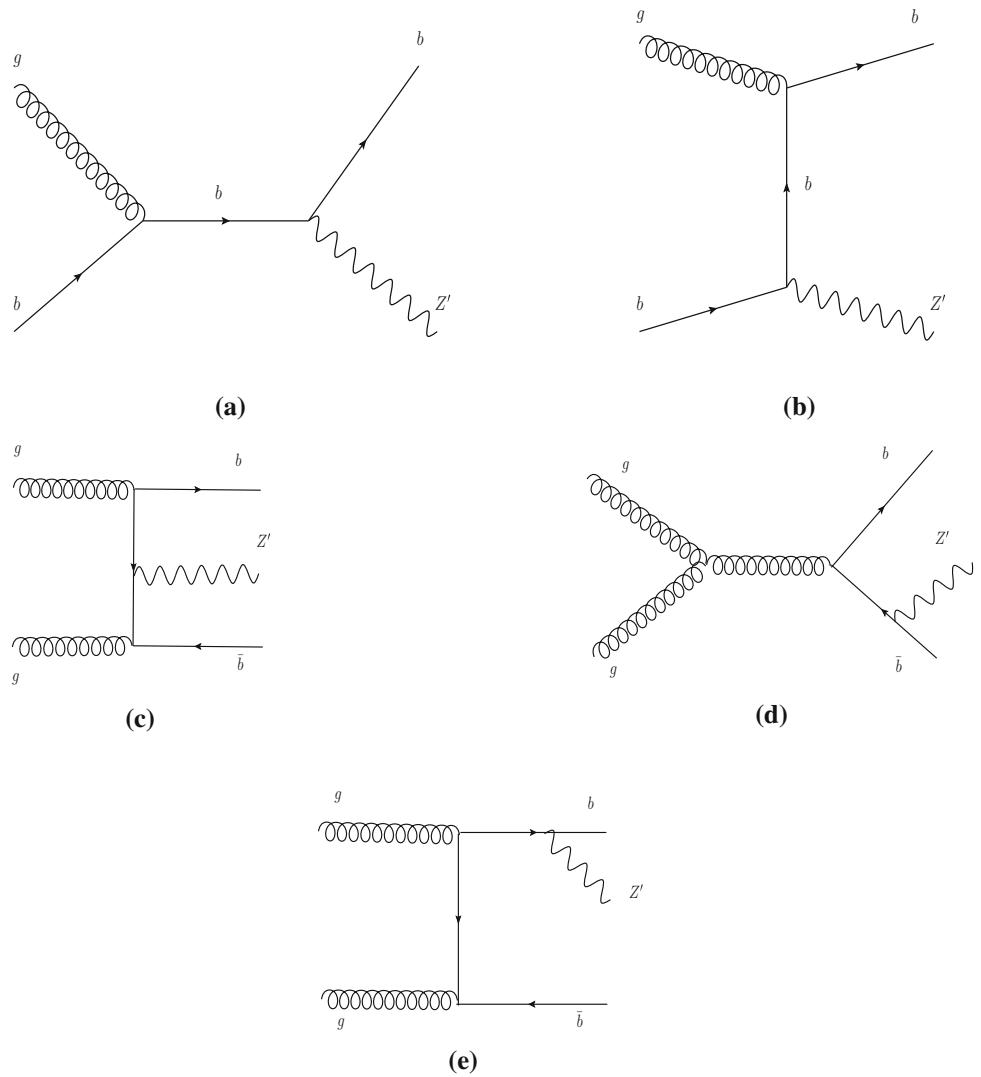
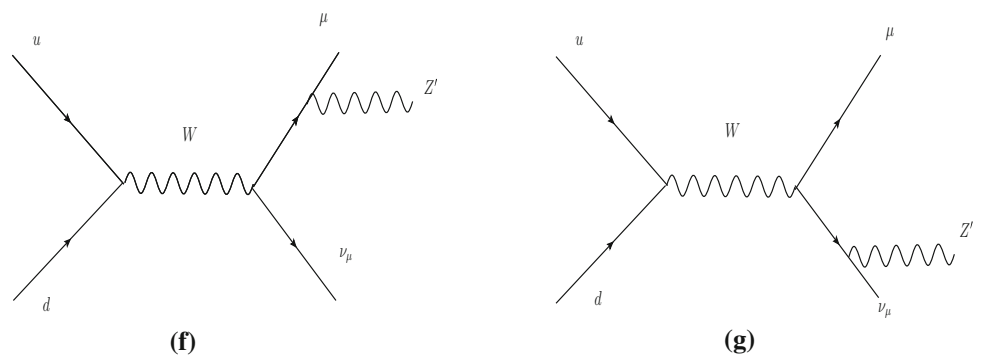


Fig. 3 Leading Feynman diagrams for the $Z' \mu^\pm E_T$ final state



the signal events these two muons originate from the decay of a heavy Z' , while for the standard model background, they originate from the Drell–Yan process, from the decay of $t(\bar{t})$ in top pair production process. For the signal, we show the distributions for two representative mass points $M_{Z'} = 200$

GeV and 500 GeV. Since the muons in the signal come from the decay of a heavy Z' , thus they are expected to have high transverse momentum. In comparison, the p_T spectrum of muons for the SM background processes are expected to peak at relatively lower values. In Fig. 5, the p_T distributions of

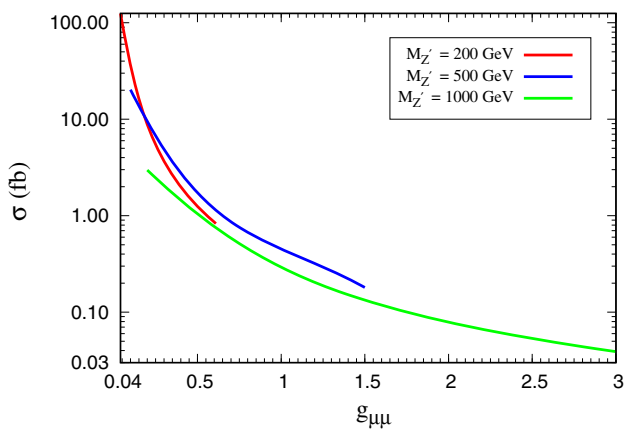


Fig. 4 The signal cross-section as a function of $g_{\mu\mu}$ for the $pp \rightarrow Z'(1b(2b) \rightarrow \mu^+\mu^- + 1b(2b)$ process. We show the results for $M_{Z'} = 200, 500$ and 1000 GeV at $\sqrt{s} = 14$ TeV. Each curve is plotted for the corresponding $g_{\mu\mu}$ range taken from Table 1, which is determined by flavor and trident constraints

the leading (μ_1) and sub-leading (μ_2) muons are contrasted between the signal and the background. We find that cutting on $p_T(\mu_1) > 90$ GeV, and $p_T(\mu_2) > 50$ GeV allows us to efficiently discriminate the signal over the SM background.

We now construct the kinematic variable R defined as a ratio of the missing transverse energy (\cancel{E}_T) to the invariant mass of the muon-pair ($M_{\mu^+\mu^-}$):

$$R = \frac{\cancel{E}_T}{M_{\mu^+\mu^-}} \tag{3.2}$$

For the signal, \cancel{E}_T can come only from p_T MISMEASUREMENT of muons and b -jets, whereas for the $t\bar{t} + jets$ background, \cancel{E}_T comes from the neutrinos in the leptonic decay of W^\pm . In Fig. 6 we show the normalized distri-

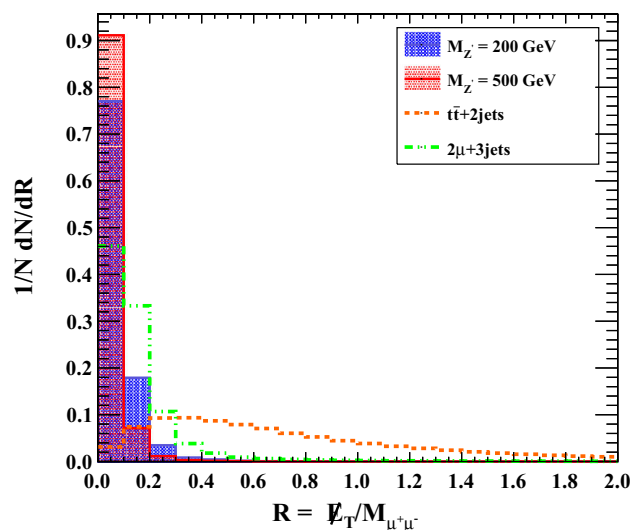


Fig. 6 Normalized $R = \frac{\cancel{E}_T}{M_{\mu^+\mu^-}}$ distribution for signal and backgrounds

bution of R . For this reason, for the signal, R peaks at a lower value while for the $t\bar{t}$ background the distribution tends to peak at a higher value of R . We find that the cut $R < 0.2$ allows one to significantly reduce the $t\bar{t} + jets$ background.

Finally we require the invariant mass of the muon pair to be in the window around the Z' peak as dictated by,

$$|M_{\mu^+\mu^-} - M_{Z'}| < 6\Gamma_{Z'},$$

where $\Gamma_{Z'}$ is the width of the Z' resonance. This cut is instrumental in further reducing the $\mu^+\mu^- + jets$ background as for these process the invariant mass of the muon pair peaks

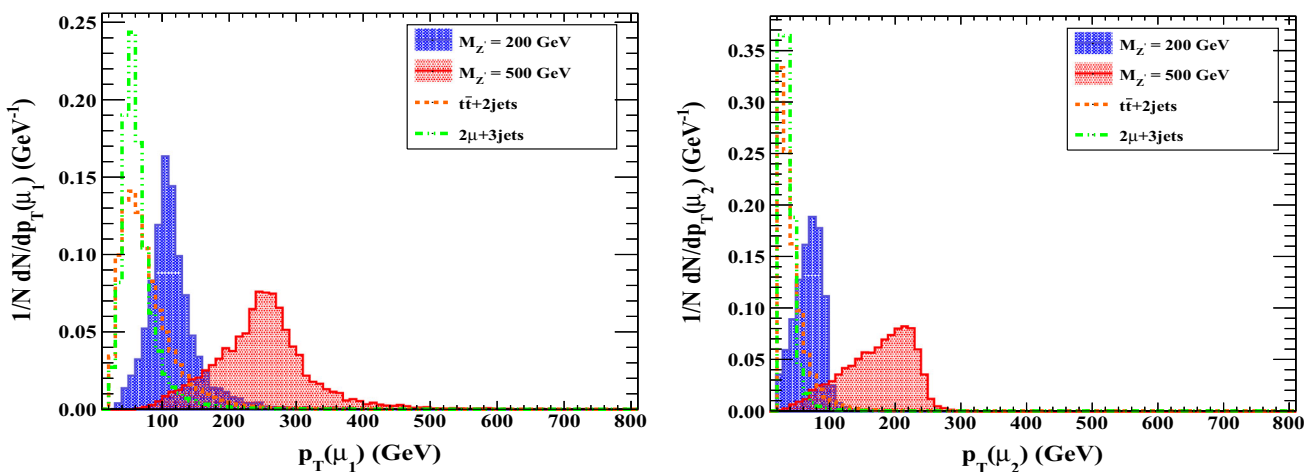


Fig. 5 Normalized transverse momentum (p_T) distributions of the leading (left) and sub-leading (right) muons for the signal ($M_{Z'} = 200$ and 500 GeV) and relevant SM backgrounds. The values of $g_{\mu\mu}$ and g_{bb} are $0.20(0.48)$ and $4.2 \times 10^{-3}(1.10 \times 10^{-2})$ for $M_{Z'} = 200(500)$ GeV, respectively

Table 2 The signal and background cross sections for the $\mu^+\mu^- + 1b(2b)$ process after each cut for $\sqrt{s} = 14$ TeV. The values of $g_{\mu\mu}$ and g_{bb} are 0.20(0.48) and $4.2 \times 10^{-3}(1.10 \times 10^{-2})$ for $M_{Z'} = 200(500)$ GeV, respectively

Process	Cross-section after cut (fb)				
	Preselection	$p_T(\mu_{1,2}) > 90(50)$ GeV	$R < 0.2$	$ M_{\mu^+\mu^-} - 200$ GeV $< 6\Gamma_{Z'}$	$ M_{\mu^+\mu^-} - 500$ GeV $< 6\Gamma_{Z'}$
$t\bar{t} + 2jets$	1861.04	264.38	78.00	3.80	1.42
$\mu^+\mu^- + 3jets$	9438.13	317.08	168.38	2.47	0.31
Total background	11299.17	581.46	246.38	6.27	1.73
Signal: $M_{Z'} = 200$ GeV	1.76	1.22	1.15	0.92	–
Signal: $M_{Z'} = 500$ GeV	0.55	0.54	0.53	–	0.39

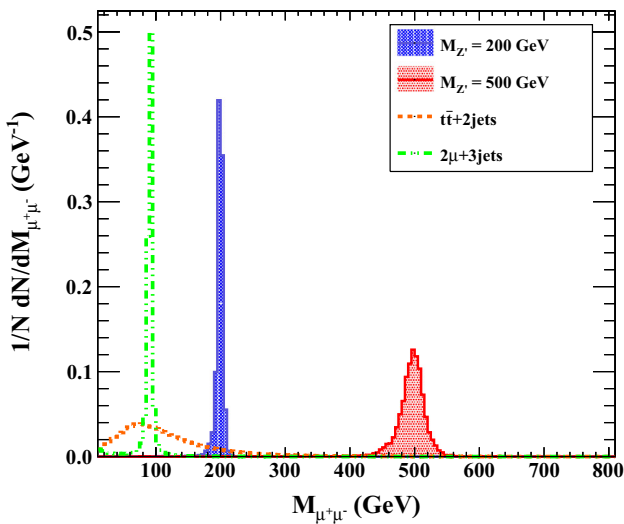


Fig. 7 Normalized invariant mass distributions of the muon-pair for signal and backgrounds

around the Z boson mass. The invariant mass distributions are depicted in Fig. 7.

Table 2 summarizes the cuts discussed above and quantifies the effect of each cut on the signal and dominant backgrounds. Using these results, the signal significance can be determined from the formula [64]

$$S = \sqrt{2 \left[(S + B) \ln \left(1 + \frac{S}{B} \right) - S \right]}, \tag{3.3}$$

where $S(B)$ are the number of signal (background) events after all the cuts. For calculating the significance, the signal and the backgrounds have been multiplied by respective k-factors to account for the next-to-leading-order (NLO) corrections. For the signal we use the k-factor of 1.38 [65], while for $t\bar{t} + jets$ and $\mu^+\mu^- + jets$ backgrounds we use the k-factors of 0.98 [66] and 1.15 [67], respectively.

Based on the results in Table 2, we can calculate the signal significance for two particular benchmark points, assuming

the integrated luminosity of $300(3000)$ fb^{-1} :

$$\begin{aligned} M_{Z'} = 200 \text{ GeV}, \quad g_{\mu\mu} = 0.20, \\ g_{bb} = 4.2 \times 10^{-3} : \quad S = 8.35 \quad (26.4), \\ M_{Z'} = 500 \text{ GeV}, \quad g_{\mu\mu} = 0.48, \\ g_{bb} = 1.1 \times 10^{-2} : \quad S = 6.8 \quad (21.5). \end{aligned} \tag{3.4}$$

These benchmarks highlight the good prospect of observing the Z' in this final state in the coming LHC runs. A broader set of results is shown in Fig. 8, where the signal significance for several representative values of $M_{Z'}$ is plotted as a function of the coupling $g_{\mu\mu}$. One can see that the discovery potential in this final state is more pronounced for lower $g_{\mu\mu}$ (which corresponds to higher g_{bb}). As expected, the discovery potential quickly diminishes with the increasing $M_{Z'}$. Nevertheless, a 5σ discovery is possible in this channel for $M_{Z'} \lesssim 500$ GeV with 300 fb^{-1} luminosity at $\sqrt{s} = 14$ TeV LHC, assuming the values of $g_{\mu\mu}$ and g_{bb} preferred by the $b \rightarrow s\mu\mu$ anomalies and allowed by low-energy constraints. In the same conditions, a 3σ discovery is possible for $M_{Z'} \lesssim 1$ TeV.

3.2 $pp \rightarrow Z'\mu^\pm + \cancel{E}_T \rightarrow 3\mu + \cancel{E}_T$ channel

We move to discussing another possible signature of the Z' particle: tri-muon plus missing energy final state. This final state arises when the Z' is radiated from μ^\pm or $\nu_\mu(\bar{\nu}_\mu)$ leg in $pp \rightarrow W^{\pm*} \rightarrow Z'\mu^\pm\nu_\mu(\bar{\nu}_\mu)$, followed by $Z' \rightarrow \mu^+\mu^-$ decay. As stated earlier, in this case both production and decay of the Z' is controlled by its coupling $g_{\mu\mu}$ to the lepton sector. Thus this channel is best suited for probing the parameter space region with relatively higher values of $g_{\mu\mu}$.

Similarly to the $\mu^+\mu^- + 1b(2b)$ analysis in the previous subsection, we generate signal events in MadGraph with the following preselection cuts:

$$\begin{aligned} \Delta R_{jj,bb,bl,jl} > 0.4, \quad R_{\ell\ell} > 0.2, \quad p_T(j, b, \ell) \\ > 10 \text{ GeV}, \quad |\eta_{j,b,\ell}| < 2.5. \end{aligned} \tag{3.5}$$

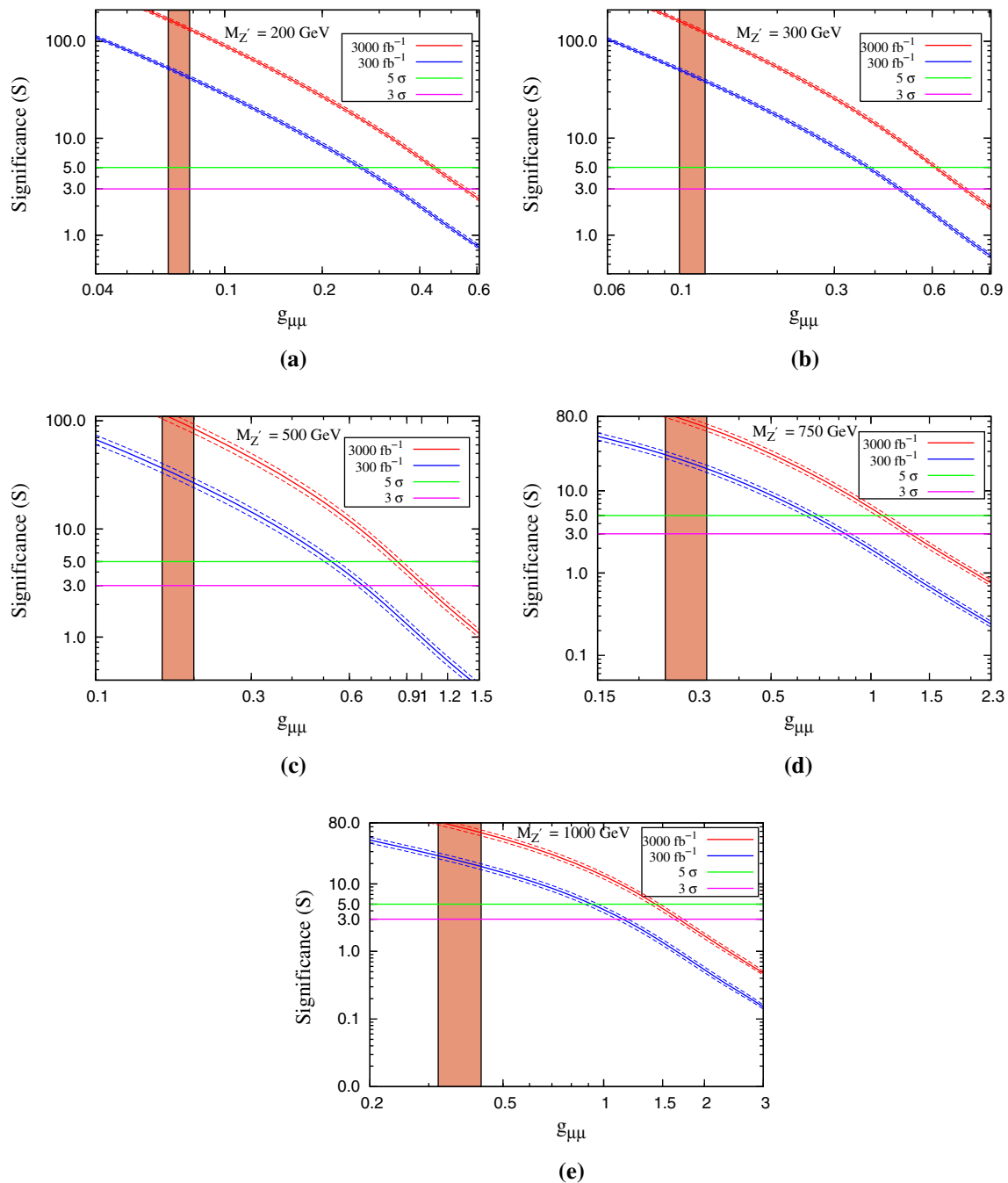


Fig. 8 Significance vs. $g_{\mu\mu}$ for $M_{Z'} = 200(8a)$, $300(8b)$, $500(8c)$, $750(8d)$ and $1000(8e)$ GeV for $\mu^+\mu^- + 1b(2b)$ channel at $\sqrt{s} = 14$ TeV. The dashed lines represent the error band in Significance curves

after including systematics $\sim 10\%$ in the background estimates. The dark shaded region is the one allowed at 1σ CL by combining the constraints from B -meson anomalies, neutrino trident and $B \rightarrow D^*\ell\nu$

In Fig. 9 we show the dependence of the leading order signal cross section of the coupling $g_{\mu\mu}$ after imposing the preselection cuts, for three representative values of $M_{Z'} = 200, 300$ and 500 GeV.

For the final state in question we can have the following SM processes that contribute to the background: WZ + jets, ZZ + jets, WW + jets, $t\bar{t}$, Z + jets. Out of these, WZ + jets and

ZZ + jets are the irreducible backgrounds. $t\bar{t}$ can contribute to the background when each top quark decays leptonically: $t \rightarrow b\nu_\mu\mu$, and the third muon arises from the semileptonic decay of one of the b -quarks. Other sub-dominant contributions arise from $t\bar{t}V$ ($V = W^\pm, Z$) or WWZ, WZZ channels [68].

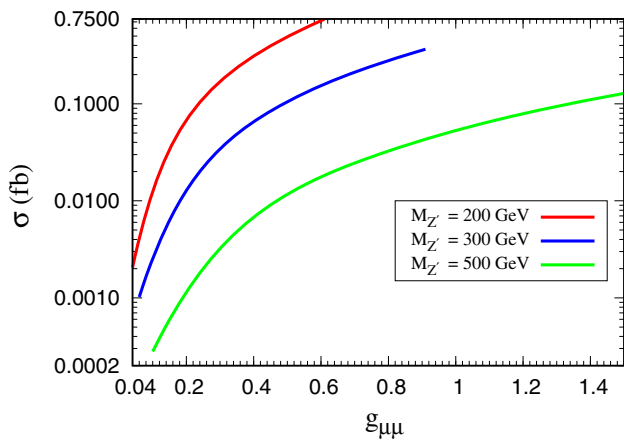


Fig. 9 Signal cross-section at $\sqrt{s} = 14$ TeV for $3\mu + \cancel{E}_T$ channel as a function of $g_{\mu\mu}$ for $M_{Z'} = 200, 300$ and 500 GeV

To optimize our signal versus background discrimination, we demand our final state to be comprised of exactly three muons with two muons of the same sign and the third muon of the opposite sign along with missing energy (\cancel{E}_T). We also impose a b -veto on the final state which helps us to reduce the $t\bar{t}$ background. For the two opposite sign dimuon pairs in the final state, we require their invariant masses, $M_{\text{OSD}}^1, M_{\text{OSD}}^2$ to satisfy

$$M_{\text{OSD}}^{1,2} < 75 \text{ GeV} \text{ or } M_{\text{OSD}}^{1,2} > 105 \text{ GeV}. \quad (3.6)$$

This helps to exclude the background contribution where the opposite sign muon pair(s) arise from Z resonance. We also impose $M_{\text{OSD}}^{1,2} > 12$ GeV to suppress the Drell–Yan back-

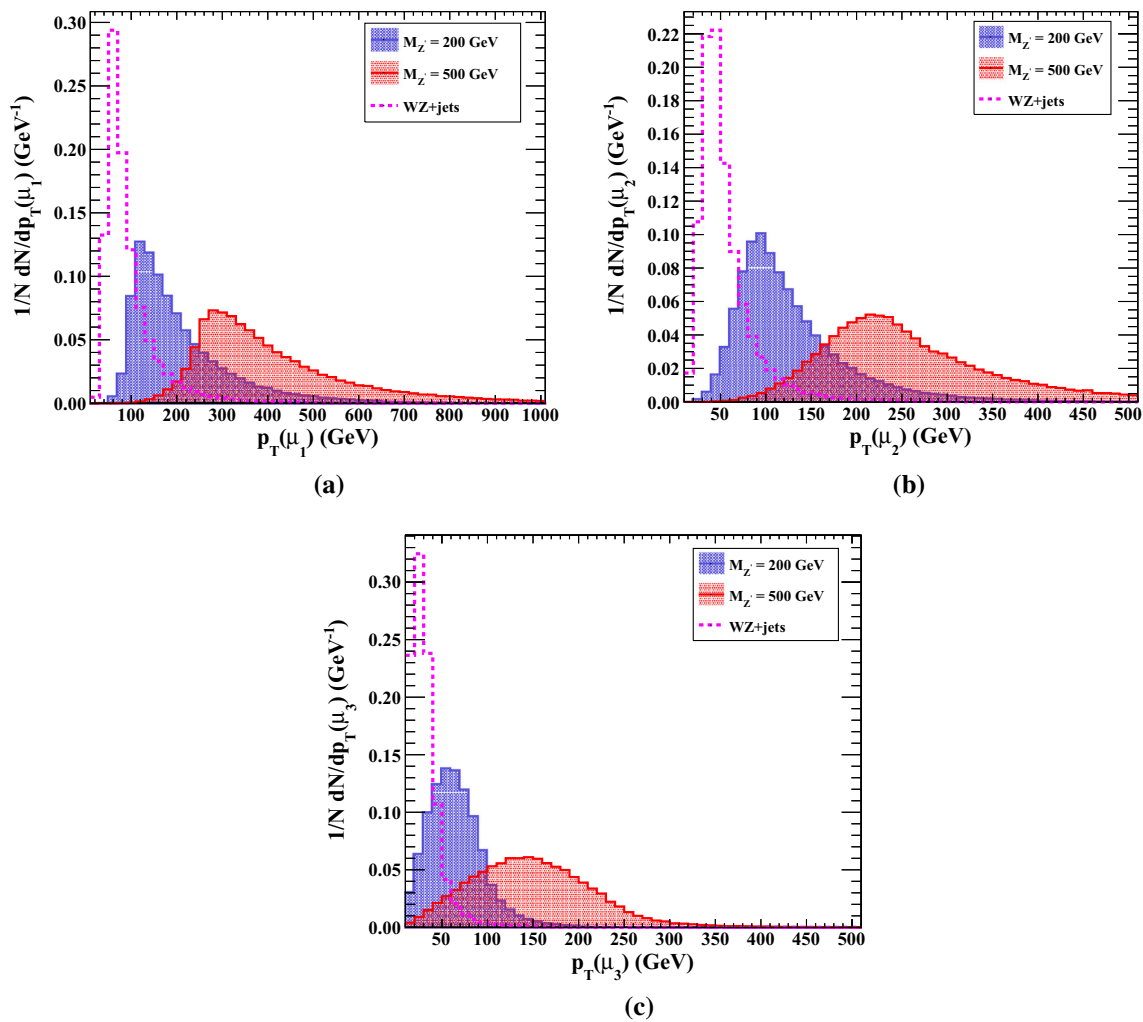


Fig. 10 Normalized transverse momentum (p_T) distributions of the leading (10a), sub-leading (10b) and sub-sub-leading (10c) muons for the $3\mu + \cancel{E}_T$ final state. Signal distributions are for $M_{Z'} = 200$ GeV,

$g_{\mu\mu} = 0.20, g_{bb} = 4.2 \times 10^{-3}$, and for $M_{Z'} = 500$ GeV, $g_{\mu\mu} = 0.48, g_{bb} = 1.10 \times 10^{-2}$. We also show the analogous distributions for the WZ background

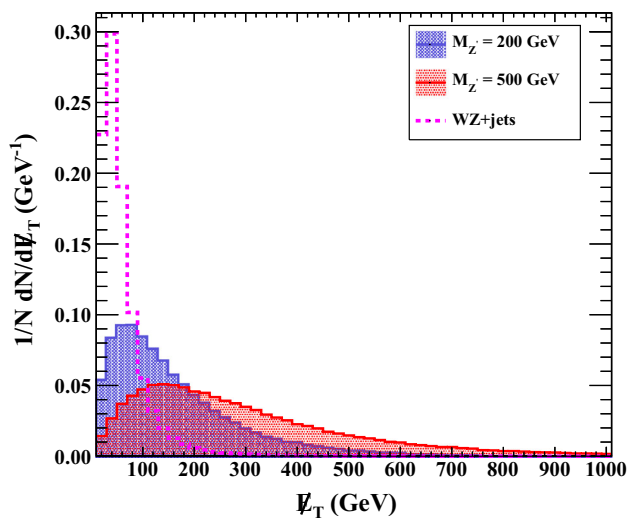


Fig. 11 Normalized missing energy (\cancel{E}_T) distribution for the $3\mu + \cancel{E}_T$ final state. We show the distribution for the signal for $M_{Z'} = 200$ GeV, $g_{\mu\mu} = 0.20$, $g_{bb} = 4.2 \times 10^{-3}$, and for $M_{Z'} = 500$ GeV, $g_{\mu\mu} = 0.48$, $g_{bb} = 1.1 \times 10^{-2}$. We also show the analogous distributions for the WZ background

ground [68]. With the above criteria, the dominantly surviving background contribution comes from WZ +jets.¹

In our analysis we assume that the Z' mass is greater than the Z and W^\pm boson masses. Thus, the muons in the signal are expected to have higher p_T than those coming from the decay of the Z or W^\pm bosons in the SM backgrounds. The comparative distributions of the transverse momenta of the the leading (μ_1), sub-leading (μ_2) and sub-sub-leading muons (μ_3) in the final state for the signal and backgrounds are shown in Fig. 10. To enhance the signal over background ratio we impose the following cuts

$$p_T(\mu_1) > 100 \text{ GeV}, \quad p_T(\mu_2) > 70 \text{ GeV}, \quad p_T(\mu_3) > 40 \text{ GeV}. \tag{3.7}$$

Finally, in Fig. 11 we compare the \cancel{E}_T distributions of signal and the WZ +jets background. The missing energy for the background comes from the leptonic decay of the W^\pm boson in WZ + jets or from mismeasurement of leptons or jets in the Drell–Yan process. As a result, the distribution of \cancel{E}_T peaks at around half of the W^\pm mass for the background, whereas for the signal it is shifted towards higher values. In our analysis we impose the cut $\cancel{E}_T > 60$ GeV which provides an optimal cut capturing the relatively long tail in the signal and avoiding the peak in the WZ +jets background.

¹ For validation, we have generated the WZ background for $\sqrt{s} = 13$ TeV using Madgraph@NLO [56] and compared with the background event expectation as given in the CMS paper [69]. Within 1σ and 2σ uncertainty of our Monte Carlo simulation, we are consistent with the CMS background numbers up to 15% and 11%, respectively.

We summarize the above discussed cut flow in Table 3 for our two representative benchmark points. Given these results, we can calculate the signal significance for our 2 benchmark points, assuming the integrated luminosity of $300(3000) \text{ fb}^{-1}$:

$$\begin{aligned} M_{Z'} = 200 \text{ GeV}, \quad g_{\mu\mu} = 0.20, \\ g_{bb} = 4.2 \times 10^{-3} : \quad S = 1.6 \text{ (5.0)}, \\ M_{Z'} = 500 \text{ GeV}, \quad g_{\mu\mu} = 0.48, \\ g_{bb} = 1.1 \times 10^{-2} : \quad S = 0.4 \text{ (1.3)}. \end{aligned} \tag{3.8}$$

The projected significance for our analysis in the $3\mu + \cancel{E}_T$ channel as a function of the coupling $g_{\mu\mu}$ is portrayed for $M_{Z'} = 200(12a)$, $300(12b)$ and $500(12c)$ GeV in Fig. 12. For the significance calculation signal and background have been scaled by k-factors of 1.25 [70] and 1.83 [71], respectively. Note that in this case, and unlike in the previously discussed $\mu^+\mu^- + 1b(2b)$ channel, the significance increases with increasing $g_{\mu\mu}$. This demonstrates the complementarity of the two final states discussed in this paper.

4 Comparison with dimuon searches

Our Z' model leads to additional LHC signatures besides those studied in Sects. 3.1 and 3.2. One is the 4 muon final state produced in the process $pp \rightarrow Z \rightarrow 4\mu$ where the Z boson decays to a muon pair and an on-shell or virtual Z' is radiated off a muon and subsequently decays into pair of muons. This is however relevant only for fairly low Z' masses, $5 \lesssim M_{Z'} \lesssim 70$ GeV [10,50,54], which are outside of our direct interest in this paper. For a heavier Z' , the strongest constraints comes from dimuon resonance searches, $pp \rightarrow Z' \rightarrow \mu^-\mu^+$ [32,42]. In our scenario, Z' is dominantly produced through its couplings to bottom quarks. Its branching fraction into muons depends on $g_{\mu\mu}$, g_{bb} and $M_{Z'}$, and it is typically significant in the interesting parameter space of the model. Other than to muons, Z' may also decay into top and bottom quarks and into neutrinos, however these channels are less competitive. In particular, we have verified that the constraints from dijet resonance searches at the LHC [72,73] are much weaker than those we obtain from the dimuon resonance searches.

Figure 13 illustrates constraints on the parameter space of the model from dimuon resonance searches. The blue band shows the range of $g_{\mu\mu}$ excluded at 95% CL by the ATLAS analysis at 13 TeV with 139 fb^{-1} of data [74,75]. We show the exclusion region for $M_{Z'} = 300$ GeV and 500 GeV, assuming the coupling g_{bb} is determined by the central value of the best fit to the $b \rightarrow s\ell\ell$ anomalies in Eq. (2.2). We can see that the regions with smaller $g_{\mu\mu}$ (hence larger g_{bb}) are disfavored; in particular the region preferred by the global fit to low-energy data is excluded by the LHC. Nevertheless,

Table 3 Effective cross-section at $\sqrt{s} = 14$ TeV for both signal and background for $3\mu + E_T$ channel after each cut described in the next . The signal benchmarks correspond to the couplings $g_{\mu\mu} = 0.20$, $g_{bb} = 4.2 \times 10^{-3}$ for $M_{Z'} = 200$ GeV, and $g_{\mu\mu} = 0.48$, $g_{bb} = 1.10 \times 10^{-2}$ for $M_{Z'} = 500$ GeV

Process	Effective cross-section after each cut (fb)			
	Preselection	$M_{OSD}^{1,2}$ cut	$p_T(\mu)$ cut	E_T cut
Background: $WZ+2j$	107.02	3.31	0.31	0.15
Signal: $M_{Z'} = 200$ GeV	6.5×10^{-2}	5.9×10^{-2}	4.4×10^{-2}	3.7×10^{-2}
Signal: $M_{Z'} = 500$ GeV	1.01×10^{-2}	9.8×10^{-3}	9.56×10^{-3}	9.0×10^{-3}

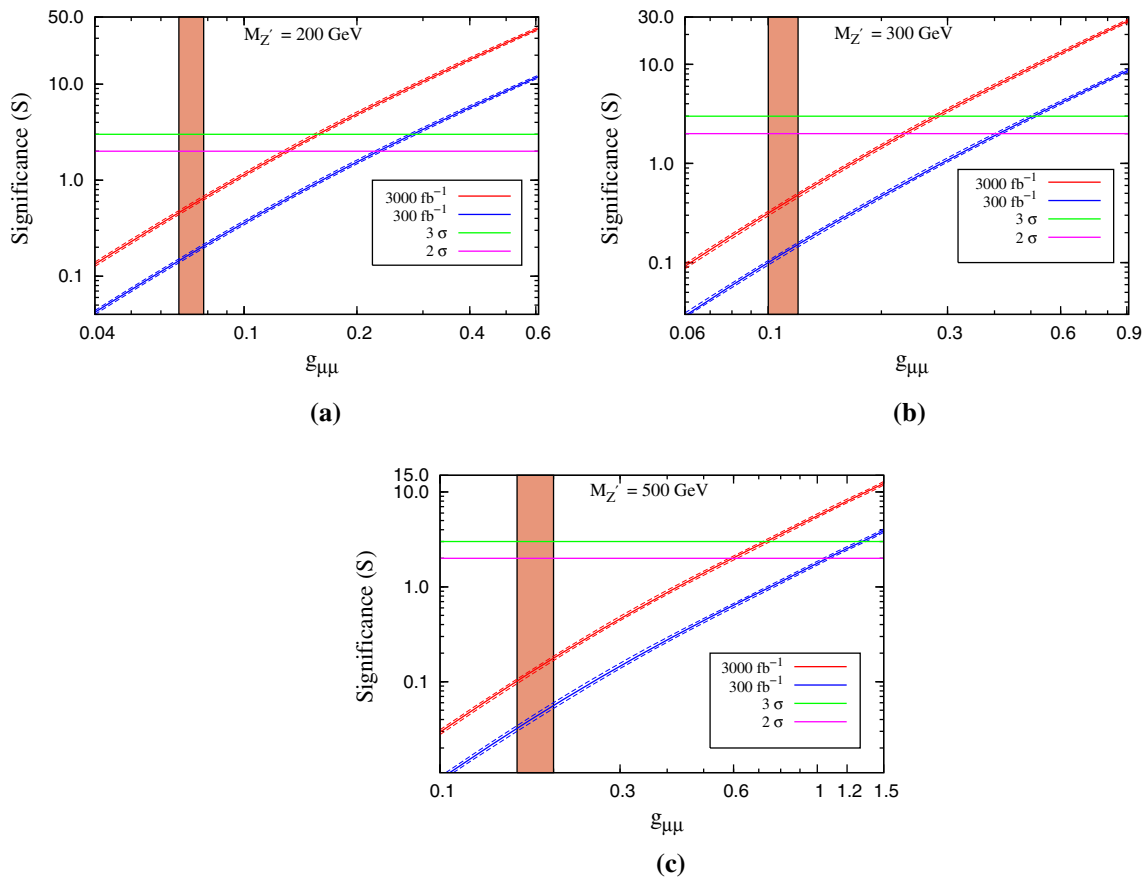


Fig. 12 Significance in the $3\mu + E_T$ channel as a function of $g_{\mu\mu}$ for $M_{Z'} = 200(12a)$, $300(12b)$ and $500(12c)$ GeV for $\sqrt{s} = 14$ TeV. The dashed lines represent the error band for the significance curves

after including systematics $\sim 10\%$ in the background estimates. The dark shaded region is the one allowed at 1σ CL by combining the constraints from B -meson anomalies, neutrino trident and $B \rightarrow D^* \ell \nu$

an important chunk of the parameter space remains allowed at 2σ by all existing LHC and low-energy analyses. Those region will be probed in the future LHC runs.

Furthermore, from Fig. 13 we learn that the dimuon and $2\mu + b$ searches probe similar regions of the parameter space, and they exhibit a similar sensitivity. This is not an accident, as the two signals are closely related, and there is an overlap between the dimuon resonance and the $2\mu + b$ signal regions. We note however that dimuon resonances are predicted by multiple new physics scenarios. Conversely, observing a signal in the $2\mu + b$ channel would be a spectacular confirmation

that the newly found resonance could explain the $b \rightarrow s\ell\ell$ anomalies.

On the other hand, in Fig. 13 we observe that the $3\mu + E_T$ process probes a complementary region of the parameter space compared to the $2\mu + b$ channel or generic dimuon resonance searches. Combining information from all of these channels will allow one to completely exclude the parameter space of our model with $M_{Z'} \lesssim 500$ GeV. Heavier Z' resonances may escape discovery at the LHC in the parameter space preferred by the $b \rightarrow s\ell\ell$ anomalies.

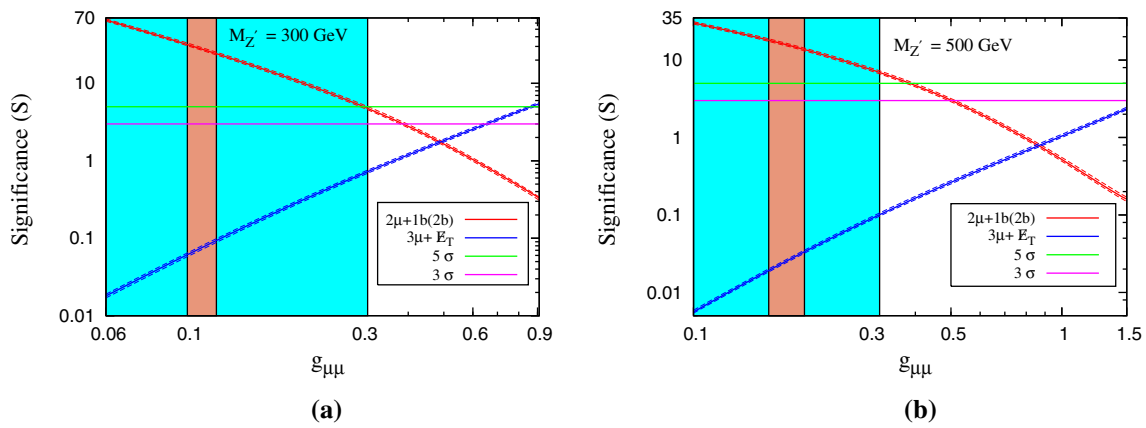


Fig. 13 The parameter range of our model excluded at 95% CL by the ATLAS dimuon resonance search [74,75] at $\sqrt{s} = 13$ TeV with 139 fb^{-1} (light blue band) for $M_{Z'} = 300$ GeV (13a) and $M_{Z'} = 500$ GeV (13b). This is compared with the signal significance expected in

the $2\mu + 1b(2b)$ (red) and $3\mu + E_T$ (blue) channels for the same collision energy and luminosity. The brown region is preferred at 1σ CL by combining the constraints from $b \rightarrow s\ell\ell$ anomalies, the neutrino trident production, and $B \rightarrow D^*\ell\nu$ processes

5 Summary and conclusions

In this work we have analyzed the LHC discovery prospects of a new massive spin-1 particle (Z') in a model explaining the $b \rightarrow s\ell^+\ell^-$ anomalies. We focused on the model proposed in Ref. [37] where tree-level exchange of the Z' contributes to $b \rightarrow s\mu^+\mu^-$ processes, and can explain in particular the apparent violation of lepton flavor universality encoded in the R_{K^*} observables. In this model the Z' has sizable couplings to left-handed bottom quarks and muons, as well as their $SU(2)_W$ partners. Therefore it can be produced on its own via $b\bar{b}$ fusion and decay into a muon pair, showing up at the LHC as a dimuon resonance. In addition, the Z' can be produced in association with another SM particle when it is radiated off a bottom, top, muon, and neutrino legs. While the dimuon resonance signature has been previously studied in this context, the associated production is less explored. In this paper we identified two promising signatures of the associated Z' production: $pp \rightarrow Z' + 1(2)b$ with Z' radiated off a bottom quark, and $pp \rightarrow Z'\mu^\pm + \cancel{E}_T$ with Z' radiated off a muon or a neutrino. In both cases we focused on Z' decays to $\mu^+\mu^-$.

The interesting parameter space of our model can be succinctly characterized by two variables: the Z' mass $M_{Z'}$, and its coupling to muons $g_{\mu\mu}$. The coupling to b-quarks g_{bb} is approximately fixed by the previous two via Eq. (2.2) as a result of fitting the $b \rightarrow s\ell^+\ell^-$ anomalies. From Eq. (2.2) g_{bb} and $g_{\mu\mu}$ are anti-correlated. We find that the $pp \rightarrow Z' + b$ channel is sensitive to lower values of $g_{\mu\mu}$, as the Z' production cross section is proportional g_{bb}^2 . This feature is the same as for Z' produced alone, and we find that these two production mechanisms offer a comparable sensitivity to the parameter space of the model. Conversely, $pp \rightarrow Z'\mu^\pm + \cancel{E}_T$ is sensitive to larger $g_{\mu\mu}$ as the Z' production cross section is

proportional $g_{\mu\mu}^2$. Taken together, the two associated production channels offer a good and complementary sensitivity to a wide range of the parameter space explaining the $b \rightarrow s\ell^+\ell^-$ anomalies for $200 \lesssim M_{Z'} \lesssim 500$ GeV.

Acknowledgements NG would like to acknowledge the Council of Scientific and Industrial Research (CSIR), Government of India for financial support. NG and SD would like to thank Professor Satyaki Bhattacharya, Abhaya Kumar Swain and Disha Bhatia for useful discussions. This work was supported in part by the CNRS LIA (Laboratoire International Associé) THEP (Theoretical High Energy Physics) and the INFRE-HEPNET (Indo-French Network on High Energy Physics) of CEFIPRA/IFCPAR (Indo-French Centre for the Promotion of Advanced Research). A.F. is partially supported by the European Union's Horizon 2020 research and innovation programme under the Marie Skłodowska-Curie Grant agreements no. 690575 and no. 674896 and Council for Scientific and Industrial Research (Grant no. 09/080(0961)/2015-EMR-I). DKG wishes to acknowledge the hospitalities of the LPT Orsay where this project was initiated and the Theoretical Physics Department, CERN, Switzerland, where part of this project was completed.

Data Availability Statement This manuscript has no associated data or the data will not be deposited. [Authors' comment: This is a phenomenological study and the work involves only MonteCarlo and Detector simulation.]

Open Access This article is licensed under a Creative Commons Attribution 4.0 International License, which permits use, sharing, adaptation, distribution and reproduction in any medium or format, as long as you give appropriate credit to the original author(s) and the source, provide a link to the Creative Commons licence, and indicate if changes were made. The images or other third party material in this article are included in the article's Creative Commons licence, unless indicated otherwise in a credit line to the material. If material is not included in the article's Creative Commons licence and your intended use is not permitted by statutory regulation or exceeds the permitted use, you will need to obtain permission directly from the copyright holder. To view a copy of this licence, visit <http://creativecommons.org/licenses/by/4.0/>.
Funded by SCOAP³.

References

1. LHCb Collaboration, R. Aaij et al., Search for lepton-universality violation in $B^+ \rightarrow K^+\ell^+\ell^-$ decays, *Phys. Rev. Lett.* **122**(19), 191801, (2019). [arXiv:1903.09252](#)
2. LHCb Collaboration, R. Aaij et al., Test of lepton universality with $B^0 \rightarrow K^{*0}\ell^+\ell^-$ decays, *JHEP* **08**, 055, (2017). [arXiv:1705.05802](#)
3. M. Algueró, B. Capdevila, A. Crivellin, S. Descotes-Genon, P. Masjuan, J. Matias, J. Virto, Addendum: “Patterns of New Physics in $b \rightarrow s\ell^+\ell^-$ transitions in the light of recent data” and “Are we overlooking Lepton Flavour Universal New Physics in $b \rightarrow s\ell\ell$?”, [arXiv:1903.09578](#)
4. M. Ciuchini, A.M. Coutinho, M. Fedele, E. Franco, A. Paul, L. Silvestrini, M. Valli, New Physics in $b \rightarrow s\ell^+\ell^-$ confronts new data on Lepton Universality. [arXiv:1903.09632](#)
5. J. Aebischer, W. Altmannshofer, D. Guadagnoli, M. Reboud, P. Stangl, D.M. Straub, B -decay discrepancies after Moriond (2019). [arXiv:1903.10434](#)
6. K. Kowalska, D. Kumar, E.M. Sessolo, Implications for New Physics in $b \rightarrow s\mu\mu$ transitions after recent measurements by Belle and LHCb. [arXiv:1903.10932](#)
7. A. Arbey, T. Hurth, F. Mahmoudi, D. Martinez Santos, S. Neshatpour, Update on the $b \rightarrow s$ anomalies. [arXiv:1904.08399](#)
8. R. Gauld, F. Goertz, U. Haisch, On minimal Z' explanations of the $B \rightarrow K^*\mu^+\mu^-$ anomaly. *Phys. Rev. D* **89**, 015005 (2014). [arXiv:1308.1959](#)
9. A.J. Buras, J. Girrbach, Left-handed Z' and Z FCNC quark couplings facing new $b \rightarrow s\mu^+\mu^-$ data. *JHEP* **12**, 009 (2013). [arXiv:1309.2466](#)
10. W. Altmannshofer, S. Gori, M. Pospelov, I. Yavin, Quark flavor transitions in $L_\mu - L_\tau$ models. *Phys. Rev. D* **89**, 095033 (2014). [arXiv:1403.1269](#)
11. A. Crivellin, G. D'Ambrosio, J. Heeck, Explaining $h \rightarrow \mu^\pm\tau^\mp$, $B \rightarrow K^*\mu^+\mu^-$ and $B \rightarrow K\mu^+\mu^-/B \rightarrow Ke^+e^-$ in a two-Higgs-doublet model with gauged $L_\mu - L_\tau$. *Phys. Rev. Lett.* **114**, 151801 (2015). [arXiv:1501.00993](#)
12. A. Crivellin, G. D'Ambrosio, J. Heeck, Addressing the LHC flavor anomalies with horizontal gauge symmetries. *Phys. Rev. D* **91**(7), 075006 (2015). [arXiv:1503.03477](#)
13. C. Niehoff, P. Stangl, D.M. Straub, Violation of lepton flavour universality in composite Higgs models. *Phys. Lett. B* **747**, 182–186 (2015). [arXiv:1503.03865](#)
14. A. Celis, J. Fuentes-Martin, M. Jung, H. Serodio, Family nonuniversal Z' models with protected flavor-changing interactions. *Phys. Rev. D* **92**(1), 015007 (2015). [arXiv:1505.03079](#)
15. A. Greljo, G. Isidori, D. Marzocca, On the breaking of lepton flavor universality in B decays. *JHEP* **07**, 142 (2015). [arXiv:1506.01705](#)
16. C. Niehoff, P. Stangl, D.M. Straub, Direct and indirect signals of natural composite Higgs models. *JHEP* **01**, 119 (2016). [arXiv:1508.00569](#)
17. W. Altmannshofer, I. Yavin, Predictions for lepton flavor universality violation in rare B decays in models with gauged $L_\mu - L_\tau$. *Phys. Rev. D* **92**(7), 075022 (2015). [arXiv:1508.07009](#)
18. A. Falkowski, M. Nardecchia, R. Ziegler, Lepton flavor non-universality in B-meson decays from a U(2) flavor model. *JHEP* **11**, 173 (2015). [arXiv:1509.01249](#)
19. A. Carmona, F. Goertz, Lepton Flavor and nonuniversality from minimal composite Higgs setups. *Phys. Rev. Lett.* **116**(25), 251801 (2016). [arXiv:1510.07658](#)
20. I. Garcia Garcia, LHCb anomalies from a natural perspective. *JHEP* **03**, 040 (2017). [arXiv:1611.03507](#)
21. E. Megias, G. Panico, O. Pujolas, M. Quiros, A natural origin for the LHCb anomalies. *JHEP* **09**, 118 (2016). [arXiv:1608.02362](#)
22. C.-W. Chiang, X.-G. He, G. Valencia, Z' model for $b \rightarrow s\ell\ell$ flavor anomalies. *Phys. Rev. D* **93**(7), 074003 (2016). [arXiv:1601.07328](#)
23. W. Altmannshofer, M. Carena, A. Crivellin, $L_\mu - L_\tau$ theory of Higgs flavor violation and $(g-2)_\mu$. *Phys. Rev. D* **94**(9), 095026 (2016). [arXiv:1604.08221](#)
24. S.M. Boucenna, A. Celis, J. Fuentes-Martin, A. Vicente, J. Virto, Phenomenology of an $SU(2) \times SU(2) \times U(1)$ model with lepton-flavour non-universality. *JHEP* **12**, 059 (2016). [arXiv:1608.01349](#)
25. P. Foldenauer, J. Jaeckel, Purely flavor-changing Z' bosons and where they might hide. *JHEP* **05**, 010 (2017). [arXiv:1612.07789](#)
26. J.F. Kamenik, Y. Soreq, J. Zupan, Lepton flavor universality violation without new sources of quark flavor violation. *Phys. Rev. D* **97**(3), 035002 (2018). [arXiv:1704.06005](#)
27. R.S. Chivukula, J. Isaacson, K.A. Mohan, D. Sengupta, E.H. Simmons, R_K anomalies and simplified limits on Z' models at the LHC. *Phys. Rev. D* **96**(7), 075012 (2017). [arXiv:1706.06575](#)
28. G. Faisel, J. Tandean, Connecting $b \rightarrow s\ell\ell$ anomalies to enhanced rare nonleptonic \bar{B}_s^0 decays in Z' model. *JHEP* **02**, 074 (2018). [arXiv:1710.11102](#)
29. J. Ellis, M. Fairbairn, P. Tunney, Anomaly-free models for flavour anomalies. [arXiv:1705.03447](#)
30. R. Alonso, P. Cox, C. Han, T.T. Yanagida, Flavoured $B - L$ local symmetry and anomalous rare B decays. *Phys. Lett. B* **774**, 643–648 (2017). [arXiv:1705.03858](#)
31. A. Carmona, F. Goertz, Recent B physics anomalies—a first hint for compositeness? [arXiv:1712.02536](#)
32. M. Abdullah, M. Dalchenko, B. Dutta, R. Eusebi, P. Huang, T. Kamon, D. Rathjens, A. Thompson, Bottom-quark fusion processes at the LHC for probing Z' models and B -meson decay anomalies. *Phys. Rev. D* **97**(7), 075035 (2018). [arXiv:1707.07016](#)
33. S. Raby, A. Trautner, A “Vector-like chiral” fourth family to explain muon anomalies. [arXiv:1712.09360](#)
34. L. Bian, S.-M. Choi, Y.-J. Kang, H.M. Lee, A minimal flavored $U(1)'$ for B -meson anomalies. *Phys. Rev. D* **96**(7), 075038 (2017). [arXiv:1707.04811](#)
35. L. Bian, H.M. Lee, C.B. Park, B -meson anomalies and Higgs physics in flavored $U(1)'$ model. [arXiv:1711.08930](#)
36. A.K. Alok, B. Bhattacharya, D. Kumar, J. Kumar, D. London, S.U. Sankar, New physics in $b \rightarrow s\mu^+\mu^-$: Distinguishing models through CP-violating effects. *Phys. Rev. D* **96**(1), 015034 (2017). [arXiv:1703.09247](#)
37. A. Falkowski, S.F. King, E. Perdomo, M. Pierre, Flavourful Z' portal for vector-like neutrino dark matter and $R_{K^{(*)}}$. *JHEP* **08**, 061 (2018). [arXiv:1803.04430](#)
38. M. Kohda, T. Modak, A. Soffer, Identifying a Z' behind $b \rightarrow s\ell\ell$ anomalies at the LHC. *Phys. Rev. D* **97**(11), 115019 (2018). [arXiv:1803.07492](#)
39. P. J. Fox, I. Low, Y. Zhang, Top-philic Z' forces at the LHC. [arXiv:1801.03505](#)
40. M. Chala, M. Spannowsky, On the behaviour of composite resonances breaking lepton flavour universality. [arXiv:1803.02364](#)
41. L. Darmé, K. Kowalska, L. Roszkowski, E.M. Sessolo, Flavor anomalies and dark matter in SUSY with an extra U(1). *JHEP* **10**, 052 (2018). [arXiv:1806.06036](#)
42. B.C. Allanach, T. Corbett, M.J. Dolan, T. You, Hadron collider sensitivity to fat flavourful Z' for $R_{K^{(*)}}$. *JHEP* **03**, 137 (2019). [arXiv:1810.02166](#)
43. P. Ko, T. Nomura, C. Yu, $b \rightarrow s\mu^+\mu^-$ anomalies and related phenomenology in $U(1)_{B_3-x_\mu L_\mu-x_\tau L_\tau}$ flavor gauge models. *JHEP* **04**, 102 (2019). [arXiv:1902.06107](#)
44. A. Biswas, A. Shaw, Reconciling dark matter, $R_{K^{(*)}}$ anomalies and $(g-2)_\mu$ in an $L_\mu - L_\tau$ scenario. *JHEP* **05**, 165 (2019). [arXiv:1903.08745](#)
45. B. C. Allanach, J.M. Butterworth, T. Corbett, Collider constraints on Z' models for neutral current B -anomalies. [arXiv:1904.10954](#)

46. A.K. Alok, A. Dighe, S. Gangal, D. Kumar, Continuing search for new physics in $b \rightarrow s\mu\mu$ decays: two operators at a time. *JHEP* **06**, 089 (2019). [arXiv:1903.09617](#)
47. J. Kawamura, S. Raby, A. Trautner, Complete vector-like fourth family and new $U(1)'$ for muon anomalies. [arXiv:1906.11297](#)
48. **CHARM-II** Collaboration, D. Geiregat et al., First observation of neutrino trident production, *Phys. Lett.* **B245**, 271–275 (1990)
49. CCFR Collaboration, S.R. Mishra et al., Neutrino trident and W Z interference. *Phys. Rev. Lett.* **66**, 3117–3120 (1991)
50. W. Altmannshofer, S. Gori, M. Pospelov, I. Yavin, Neutrino trident production: a powerful probe of new physics with neutrino beams. *Phys. Rev. Lett.* **113**, 091801 (2014). [arXiv:1406.2332](#)
51. A. Falkowski, M. González-Alonso, K. Mimouni, Compilation of low-energy constraints on 4-fermion operators in the SMEFT. *JHEP* **08**, 123 (2017). [arXiv:1706.03783](#)
52. **CKMfitter Group** Collaboration, J. Charles, A. Hocker, H. Lacker, S. Laplace, F.R. Le Diberder, J. Malcles, J. Ocariz, M. Pivk, L. Roos, CP violation and the CKM matrix: Assessing the impact of the asymmetric B factories, *Eur. Phys. J.* **C41**(1), 1–131, (2005). [arXiv:hep-ph/0406184](#)
53. S. Descotes-Genon, A. Falkowski, M. Fedele, M. González-Alonso, J. Virto, The CKM parameters in the SMEFT. *JHEP* **05**, 172 (2019). [arXiv:1812.08163](#)
54. W. Altmannshofer, S. Gori, S. Profumo, F.S. Queiroz, Explaining dark matter and B decay anomalies with an $L_\mu - L_\tau$ model. *JHEP* **12**, 106 (2016). [arXiv:1609.04026](#)
55. A. Alloul, N.D. Christensen, C. Degrande, C. Duhr, B. Fuks, FeynRules 2.0—A complete toolbox for tree-level phenomenology. *Comput. Phys. Commun.* **185**, 2250–2300 (2014). [arXiv:1310.1921](#)
56. J. Alwall, R. Frederix, S. Frixione, V. Hirschi, F. Maltoni, O. Mattelaer, H.S. Shao, T. Stelzer, P. Torrielli, M. Zaro, The automated computation of tree-level and next-to-leading order differential cross sections, and their matching to parton shower simulations. *JHEP* **07**, 079 (2014). [arXiv:1405.0301](#)
57. **NNPDF** Collaboration, R.D. Ball et al., Parton distributions for the LHC Run II, *JHEP* **04**, 040, (2015). [arXiv:1410.8849](#)
58. T. Sjostrand, S. Ask, J.R. Christiansen, R. Corke, N. Desai, P. Ilten, S. Mrenna, S. Prestel, C.O. Rasmussen, P.Z. Skands, An introduction to PYTHIA 8.2. *Comput. Phys. Commun.* **191**, 159–177 (2015). [arXiv:1410.3012](#)
59. **DELPHES 3** Collaboration, J. de Favereau, C. Delaere, P. Demin, A. Giammanco, V. Lemaitre, A. Mertens, M. Selvaggi, DELPHES 3, A modular framework for fast simulation of a generic collider experiment, *JHEP* **02**, 057 (2014). [arXiv:1307.6346](#)
60. M. Cacciari, G.P. Salam, G. Soyez, The anti- k_t jet clustering algorithm. *JHEP* **04**, 063 (2008). [arXiv:0802.1189](#)
61. M.L. Mangano, M. Moretti, F. Piccinini, M. Treccani, Matching matrix elements and shower evolution for top-quark production in hadronic collisions. *JHEP* **01**, 013 (2007). [arXiv:hep-ph/0611129](#)
62. S. Hoeche, F. Krauss, N. Lavesson, L. Lonnblad, M. Mangano, A. Schalicke, S. Schumann, Matching parton showers and matrix elements, in *HERA and the LHC: A Workshop on the implications of HERA for LHC physics: Proceedings Part A*, pp. 288–289, (2005). [arXiv:hep-ph/0602031](#)
63. C.M.S. Collaboration, S. Chatrchyan et al., Identification of b-quark jets with the CMS experiment. *JINST* **8**, P04013 (2013). [arXiv:1211.4462](#)
64. G. Cowan, K. Cranmer, E. Gross, O. Vitells, Asymptotic formulae for likelihood-based tests of new physics. *Eur. Phys. J. C* **71**, 1554 (2011). [arXiv:1007.1727](#). **Erratum: Eur. Phys. J. C73,2501(2013)**
65. J.M. Campbell, R.K. Ellis, F. Maltoni, S. Willenbrock, Production of a Z boson and two jets with one heavy-quark tag. *Phys. Rev. D* **73**, 054007 (2006). [arXiv:hep-ph/0510362](#). **Erratum: Phys. Rev.D77,019903(2008)**
66. **NLO Multileg Working Group** Collaboration, Z. Bern et al., The NLO multileg working group: Summary report, in *Physics at TeV colliders, La physique du TeV aux collisionneurs, Les Houches 2007 : 11–29 June 2007*, pp. 1–120, 2008. [arXiv:0803.0494](#)
67. S. Catani, L. Cieri, G. Ferrera, D. de Florian, M. Grazzini, Vector boson production at hadron colliders: a fully exclusive QCD calculation at NNLO. *Phys. Rev. Lett.* **103**, 082001 (2009). [arXiv:0903.2120](#)
68. C.M.S. Collaboration, S. Chatrchyan et al., Search for anomalous production of events with three or more leptons in pp collisions at $\sqrt{s} = 8$ TeV. *Phys. Rev. D* **90**, 032006 (2014). [arXiv:1404.5801](#)
69. C.M.S. Collaboration, A.M. Sirunyan et al., Search for electroweak production of charginos and neutralinos in multilepton final states in proton-proton collisions at $\sqrt{s} = 13$ TeV. *JHEP* **03**, 166 (2018). [arXiv:1709.05406](#)
70. **ATLAS** Collaboration, T.A. collaboration, Search for doubly-charged Higgs bosons in same-charge electron pair final states using proton–proton collisions at $\sqrt{s} = 13$ TeV with the ATLAS detector, ATLAS-CONF-2016-051
71. M. Grazzini, S. Kallweit, D. Rathlev, M. Wiesemann, $W^\pm Z$ production at hadron colliders in NNLO QCD. *Phys. Lett. B* **761**, 179–183 (2016). [arXiv:1604.08576](#)
72. **ATLAS** Collaboration, M. Aaboud et al., Search for new phenomena in dijet events using 37 fb^{-1} of pp collision data collected at $\sqrt{s} = 13$ TeV with the ATLAS detector, *Phys. Rev.* **D96**(5), 052004 (2017). [arXiv:1703.09127](#)
73. **CMS** Collaboration, C. Collaboration, Searches for dijet resonances in pp collisions at $\sqrt{s} = 13$ TeV using data collected in 2016, CMS-PAS-EXO-16-056
74. **ATLAS** Collaboration, T.A. collaboration, Search for high-mass dilepton resonances using 139 fb^{-1} of pp collision data collected at $\sqrt{s} = 13$ TeV with the ATLAS detector, ATLAS-CONF-2019-001
75. **ATLAS** Collaboration, G. Aad et al., Search for high-mass dilepton resonances using 139 fb^{-1} of pp collision data collected at $\sqrt{s} = 13$ TeV with the ATLAS detector. [arXiv:1903.06248](#)